Development of hybrid façade panels in prestressed stone and eco-efficient concrete

João Carlos Revés Pereira da Silva

May 2019

Abstract

Nowadays, the construction sector seeks, not only the adoption of constructive solutions that allow a significant saving of time and costs, but that also comply with an eco-efficiency component. This dissertation was developed following the "*INOVWALL*" project, with the cooperation of Frontwave, whose purpose is to create a facade panel system that is functional and also seeks to comply with the eco-efficiency requirement. In the process of cutting natural stone in the factory (after extraction in the field), it is estimated that significant wastes are originated, circa of 60%. In order to value the limestone waste from a stone processing company, it will be incorporated in concrete as aggregate, which will later be used in the production of facade panels. The hybrid panel concept involves creating a two-face system in which the outer face will be composed by stone plates (higher quality solution) and the inner plate will be made with the concrete produced, in order to recycle the waste originated by the stone industry. The formulation of this concrete has the purpose of creating an economically competitive solution, being simultaneously a solution with less environmental impact. The prestress will be applied both on the stone plate and on the concrete plate, to connect both faces.

Key-words

Facade, Panel, Eco-efficient, Hybrid, Prestress

1. Introduction

The cladding of buildings is an aspect that has been gaining more importance, since it is an aspect of the global project of buildings that directly affects the aesthetic characteristics of facades. Nowadays, the construction market seeks not only the adoption of constructive solutions that allow a significant saving of time and costs, but that also comply with an eco-efficiency component.

2. State of art

The industry of stone has increased in the latest years with the development of different solutions of cladding, giving an extra value to the material of natural stone. However, one of the main concerns regarding this industry is the production of high quantities of stone waste in its transformation. The waste is originated in different stages of the stone processing, as represented in Figure 1.

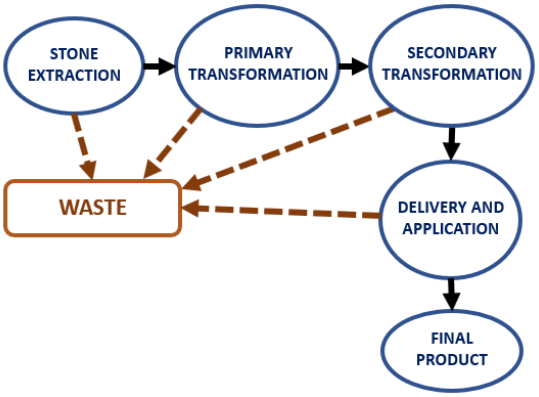

Figure 1 – Production of stone waste

In this study, the waste of limestone was used in the production of recycled aggregate.

3. Concept

The concept of the panel was to create a product that is viable for façade cladding or to serve as wall. In this case, the hybrid panel makes use of three different components that are essential to its definition: natural stone, concrete and prestress.

3.1. Natural stone

The type of stone used for the outer plates and for the aggregate production was a type of limestone, called “moca-creme”. This stone is used in both outer and inner faces of the hybrid panel. The outer face of the panel is composed by three individual plates of “moca-creme” limestone. The three plates will be glued with an epoxy resin, applied throughout its thickness of 30 mm. The dimensions of each plate are 0,6x0,5x0,03 (m^3). The top two plates have a space to receive the anchor plates, which will occupy both ends of each panel. In Figure 2 and 3, it is represented a draw of each stone plate (intermedium and top plates, respectively). The characteristics of the stone are presented in Table 1.

Figure 2 – Draw of an intermedium plate

Figure 3 – Draw of a top plate

Table 1 – Stone characterization

Compression strength	93 MPa
Tensile flexural strenght	9,4 MPa
Density	2430 kg/m^3
Young modulus	45 GPa

3.2. Concrete

The inner face uses a single concrete plate, produced with “moca-creme” limestone aggregate. The production of one single concrete plate had to make its dimensions compatible with the outer face. In order to achieve that, two wood formworks were constructed, to produce concrete plates, each with a total dimension of 1,5x0,6x0,03 (m) and two spaces at both ends of the plate, to place the anchor plates. The formulation of the concrete had to consider that the concrete plate must present the same level of deformations as in the stone plate. In order to achieve that purpose, the Young modulus of concrete and stone should be similar. Table 2 shows the Young modulus values for each material used to produce the panel.

Table 2 – Young Modulus of stone and concrete

Material	E (GPa)
Limestone	45
Concrete	35

Although these values should be similar, the production of a concrete with the same Young modulus of the stone would require a high strength C90/105 class concrete (according to EC2), which would require the use of unnecessary high dosages of cement in the concrete production. The deformation values of each material will be presented later, showing that the choice of producing a concrete with this Young modulus didn’t create any problem in terms of length compatibilization of each plate of the panel. Since the concrete plate has only a 30 mm thickness, it would be very difficult to vibrate the concrete. For that reason, it was produced a self-compacting concrete.

3.3. Prestress

The prestress was introduced in the panel to connect both materials. Each end of the panel as an anchor plate with three holes. A Φ6 wire made of 1670/1860 steel is introduced in each hole, in order to introduce the prestress strength in the panel. To evaluate the effect of prestress in the cross section of the panel, a normal stress diagram is represented in Figure 4.

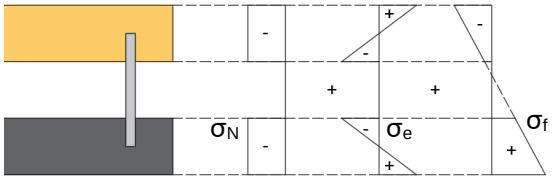

Figure 3 – Normal stress diagrams

Since both materials will only be connected when the prestress strength is installed, the eccentric component of prestress will cause both plates to bend individually, with their own bending modulus (w_1). The following expression was used to calculate the bending modulus of one plate:

$$w_1 = \frac{I_{plate}}{z^*} = \frac{\frac{600 \times 30^3}{12}}{15} = 90000\ mm^3$$

When the concrete and limestone plates start to bend together (after prestress is introduced), a different bending modulus can be considered (w_2) for the external loads of the panel. The following expression was used to calculate the normal stress in the lower fibre of the bottom plate. The prestress strength in each plate has an eccentricity of 5 mm (e).

$$\sigma = -\sigma_N + \sigma_e + \sigma_f = -\frac{N^*}{A} + \frac{N^* \times e}{w_1} + \frac{M}{w_2} =$$
$$= -\frac{N^*}{18000} + \frac{N^* \times 5}{90000} + \frac{M}{w_2} = \frac{M}{w_2}$$

After applying the expression above, it is possible to conclude that the prestress strength only acts as a way of connecting the plates. Unlike the cases of prestressed concrete structures where the flexural strength is increased by the eccentric diagram (σ_e), in this case, the sum of the eccentric and uniform (σ_N) components of prestress always lead to a null stress in the lower fiber of the bottom plate, regardless the level of prestress that was installed in the panel. To prevent the panel from buckling, the buckling loads (P_{cr}) were calculated for each plate of the panel (limestone and concrete), using the following expression:

$$P_{cr} = \frac{\pi^2 EI_{plate}}{{L_{cr}}^2}$$

Since the plates have different materials with different Young modulus, it was necessary to calculate the buckling load considering the relative axial stiffness (K_r), by using the following expression:

$$K_i = \frac{E_i \times A_i}{\sum_{j=1}^{n}(E_j \times A_j)}$$

The results are presented in Table 3. The load P* is the buckling strength in each wire.

Table 3 – Buckling loads for each plate

Material	P* (kN)
Limestone	148
Concrete	148

Since a strength of approximately 52 kN is needed to reach the steel characteristic stress (f_{pk}) in each wire, it's not possible to reach higher loads (Table 3). For that reason, buckling will not be a problem in this panel. The load used in each wire was defined as half of the steel characteristic strength (≈ 25 kN). The prestressing system used to connect the panel is represented in Figure 4.

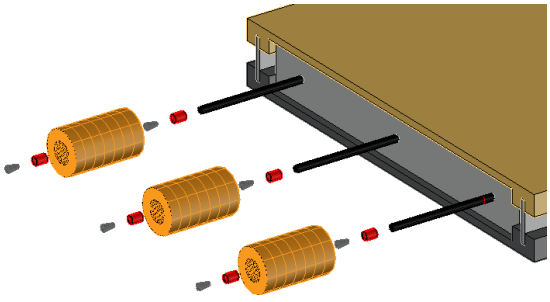

Figure 4 – Prestress scheme in exploded view

4. Experimental characterization

The experimental characterization of the panels included the four following stages:

i. Aggregate production;
ii. Concrete production and characterization;
iii. Panels production and assembly;
iv. Panels flexural tests.

4.1. Aggregate production

The aggregate resulted from the crushing of stone waste produced by the stone industry. This process allows the waste recovery, to create a new product that is more environmentally friendly. The stone used to produce the aggregate was the same from the outer surface, the “moca-creme” limestone. The resultant product of the crushing process is a mix of aggregates, with a variety of dimensions, from (thin aggregates, to thicker ones). Since the concrete plates will be produced with a thickness of 30mm, it is important to establish a limit to the maximum dimensions of the aggregates. The limit of the aggregate dimensions was defined as $1/3$ of the thickness of the concrete plate (10 mm). To assure that the particles in the aggregate mixture respect that dimension limit, a sifting process is required. This process also allowed to obtain the particle size distribution curve. The equipment used in the production and characterization of the aggregate is shown in Figure 5: (a) stone crusher; (b) coarse aggregate sieve; (c) thin aggregate sieve.

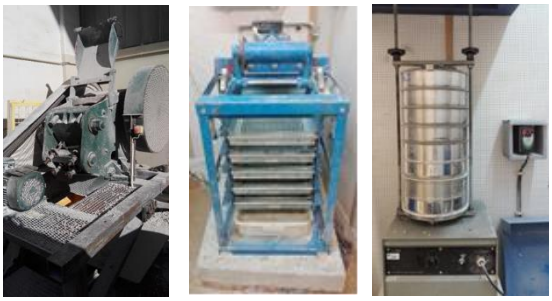

(a) (b) (c)

Figure 5 – Crushing and sifting equipment

Before starting the sifting process, a series of sieves were previously defined. The chosen series was the European series. The results from the sifting process were used to obtain the grain size particle curve. To see if any addition of aggregate was needed, a reference Faury curve was defined. For a self-compacting concrete with crushed aggregates, the parameters to draw the curve were defined as A = 43 and B = 2. Figure 6 shows the Faury reference curve (red) and the grain size particle curve (brown). The horizontal axis refers to the dimension of the grains and the vertical axis refers to the percentage of material that passed through the meshes.

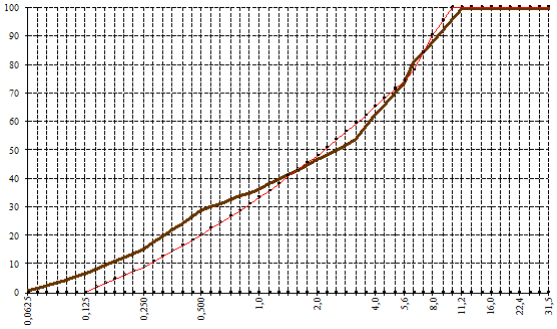

Figure 6 – Faury and grain size particle curves

The graphic shows that the grain size particle curve as a higher fine content than the Faury curve, for aggregates with dimension lower than 2 mm. For larger aggregate dimensions, the particles distribution is very similar in both curves.

4.2. Concrete formulation

The definition of the concrete formulation involved the following steps:

i. Specification of strength and density of concrete and selection of all components in the final mixture;
ii. Prediction of concrete compactness, which mainly depends on the type and dosage of the binding powders and admixtures and on the shape and maximum size of aggregates;

iii. Quantification of the binding paste, through the dosages of the binging powders (cement and limestone filer) and estimative of the compactness and of the air volume of that paste;

iv. Verification of the adjustment of the grain size particle curve to the Faury curve;

v. Prevision of the binding paste strength ($f_{c,j}$) through the Feret's expression, which relates that strength with the compactness of the paste (γ) and the Feret coefficient ($k_{1,j}$) at age of *j* days;

$$f_{c,j} = k_{1,j} \times \gamma^2$$

vi. Prediction of the concrete's strength through a coefficient (C_f) that considers the type (and dosage) of the aggregate;

$$f_c = f_{c,j} \times C_f$$

$$C_f = \prod_{i=1}^{n} \left(1 - \frac{V_{abs,i}}{100} \times 0{,}20 \times 0{,}51^{\rho_{Po,i}{}^{2,9}}\right)$$

vii. Setting the concrete mixture design dosages with both volumetric and mass proportions of the constituents.

After applying all the steps described above, the final mixture can be defined as presented in Table 4.

Table 4 – Concrete composition

Material	Designation	Fraction (kg/m³)
Aggregate	Limestone	1616
Cement	CEM I 52,5R	300
Adjuvant	Limestone Filer	270
Superplasticizer	Master Glenium 526	5,3
Water	-	155
Absorption water	-	40

In order to characterise the concrete, different test were made to evaluate the concrete density, compressive strength, tensile strength and Young modulus. The results for each of these parameters is presented in Table 5.

Table 5 – Concrete characterization

Parameter	Concrete age (days)	Value
ρ	-	2360kg/m³
f_{cm}	7	51,6 MPa
	28	60,6 MPa
f_{ct}	28	3,27 MPa
f_{ctf}	1	5,6 MPa
	7	7,7 MPa
	28	8,9 MPa
E	28	26 GPa

4.3. Panels production and assembly

The first step to produce the panels was the production of concrete plates, by following the mixture composition described in Table 5. The concrete plates are then placed horizontally, and two aluminium profiles are glued on both sides of the plate with epoxy resin. The prestress system is assembled in the panel, by placing the anchor plates with the prestress wires on both extremities of the panel. For each wire, two wedges and barrels were fixed on each extremity. After that, three stone plates (Figures 2 and 3) were placed on top, by fitting the aluminium profiles in the grooves of those plates. A thin layer of epoxy resin was also used in this step, to glue the intermediate plate to the top plates. To finish the assembly of all materials, a prestress system with three hydraulic jacks was used. The result of the panels production and assembly is presented in Figure 7, with a scheme in exploded view showing the way each material fits in the final panel.

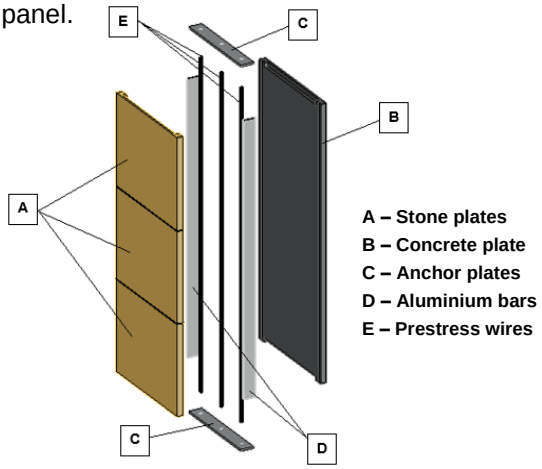

Figure 7 – Production and assembly of one hybrid panel

5. Panels flexural tests

The panels were tested with two linear loads applied at 1/3 and 2/3 of the total length of the panel. The force actuator was primarily coupled to a HEB 240 profile. Two HEB 100 profiles were later screwed to the HEB 240. With the force transmitted from the actuator, those profiles will transmit that force to the panel through two wood rulers, which allow the setup to create two linear loads. The panel was supported at four different points. Each support was 4 cm away from the edges of the panel. A total of five LVDT (Linear Variable Differential Transformer) were used to obtain the displacements along the length (1,42 meters). In Figure 8, it is represented the setup to perform the tests.

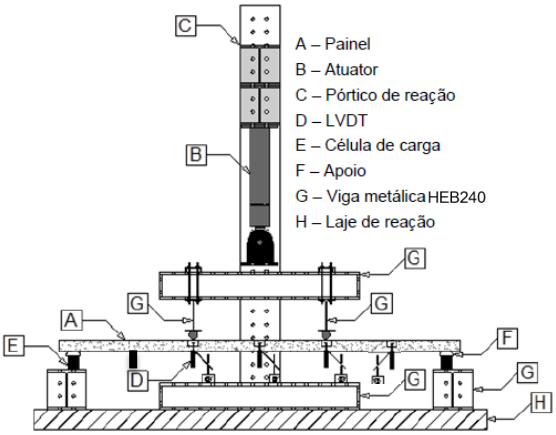

Figure 8 – Tests setup (Ferreira, 2015)

Each LVDT was placed in order to measure the vertical displacements on each 25 cm of the panel. The cross sections where the displacements were measured are represented in Figure 9.

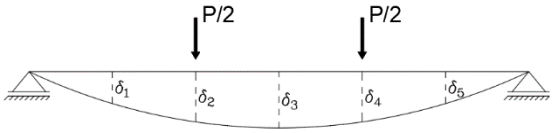

Figure 9 – Displacements measured

A total of four panels were tested. The flexural tests of three panels were divided in two stages: loading and unloading in different levels of force and loading until a failure mode is observed. In the first stage, the panels were loaded with force control, as a way of evaluating the elastic behaviour of the panels. In the second stage, the panels were loaded with displacement control, until the first failure was observed. Two panels were loaded in the concrete plate and the other was loaded in the stone plate. In the remaining panel, only the first stage of the tests was made (to evaluate the elastic behaviour), by applying the load in the stone plate.

5.1. Estimative of failure

For each scheme, it was calculated the loads in the actuator that produce different failure modes. The failure modes for each test scheme are represented in Figure 10.

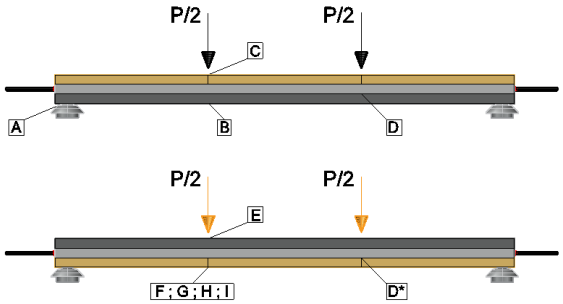

A – Concrete shear
B – Concrete fracturing
C – Stone crush
D – Aluminium yield
D* – Aluminium yield
E – Concrete smashing
F – Stone fracturing
G – Resin tensile stress
H – Resin shear
I – Stone shear

Figure 10 – Possible failure modes

The loads for each failure mode described above were calculated. For failures B, C, D, D*, E, F and G, the following expressions were used to calculate the support reactions and the loads in the actuator (P*), depending on the materials resistances (and considering an elastic behaviour):

$$\frac{0{,}6 \times 0{,}03 \times 1{,}5 \times (24{,}3 + 23{,}6)}{4} \approx 0{,}32\ \text{kN}$$

$$P^* = \left[\left(\frac{\sigma_{máx.} \times w_2}{460}\right) \times 10^{-3} - 2 \times 0{,}32\right] \times 2$$

The loads results for the failure modes B to G are presented in Table 6.

Table 6 – Actuator loads for failure modes B to G

Failure	$\sigma_{máx.}$ (MPa)	w_2 (mm^3)	P* (kN)
B	3,3	7,06 x 10^5	10,1
C	93	7,06 x 10^5	284
D	100	9,84 x 10^5	426,6
D*	100	1,7 x 10^6	737,8
E	40	1,01 x 10^6	174,4
F	9,4	1,01 x 10^6	40
G	20	1,01 x 10^6	86,6

For the failure modes H and I, the following expression was used to calculate the maximum shear in the load cross section, depending on the shear resistances of limestone and resin.

$$V = \frac{\tau_i \times t \times \sum_{j=1}^{n} E_j I_j}{\sum_{i=1}^{n} E_i S_i}$$

The loads results for the failure modes H and I are presented in Table 7. The loads in the actuator are represented by P, after deducting the support reactions

Table 7 – Actuator loads for failure modes B to G

Material	τ (MPa)	E (GPa)	I (mm^4)
Aluminium	-	70	2,73×10^7
Concrete	-	26	1,1×10^6
Limestone	5,5	45	1×10^7
Resin	17	5,5	-
Material	**S (mm^3)**	**V (kN)**	**P (kN)**
Aluminium	-	-	-
Concrete	-	-	-
Limestone	1,1 × 10^6	3,9	7,8
Resin	1,1 × 10^6	32,1	64,2

For the failure mode A, the following expressions were used to calculate the concrete shear resistance ($V_{Rd,c}$) according to EC2.

$$v_{Rd,c} = C_{Rd,c} k (100 \rho_l f_{ck})^{1/3} + k_1 \sigma_{cp} \geq v_{min} + k_1 \sigma_{cp}$$

Since the concrete plate was not reinforced with steel, the geometric percentage of steel (ρ_l) in the cross section is null. For that reason, the concrete shear resistance is equal to to the minimum resistance of the non-reinforced concrete (v_{min}) plus the effect of the uniform compressive stress of prestress ($k_1\sigma_{cp}$).

$$v_{min} = 0{,}035 k^{3/2} {f_{ck}}^{1/2}$$

$$k = 1 + \sqrt{\frac{200}{d}} \leq 2 \Longrightarrow k = 1 + \sqrt{\frac{200}{30}} > 2 \Longrightarrow k = 2$$

$$v_{min} = 0{,}035 \times 2^{3/2} \times 40^{1/2} \approx 0{,}626 \text{ MPa}$$

$$\sigma_{cp} = \frac{20000 \times 3 \times 0{,}366}{600 \times 30} = 1{,}22 < 0{,}2 \times \frac{40}{1{,}5} \approx 5{,}3$$

After calculating v_{min} and σ_{cp}, the concrete shear resistance is obtained by considering an effect of 10% of the uniform compressive stress (k_1=1).

$$v_{Rd,c} = v_{min} + k_1 \sigma_{cp} =$$
$$= 0{,}035 \times 2^{3/2} \times 40^{1/2} + 0{,}1 \times 1{,}22 = 0{,}748 \text{ MPa}$$

Considering the calculus of the shear force in a concrete slab, the following expression was used to obtain the force of the actuator, for this failure mode to occur. According to EC2, an increasing factor β = 1,5 may be considered for eccentric supports in a slab. After calculating the concrete shear resistance, the force in the actuator (P*) may be obtained by deducting the support reaction.

$$V_{sd} = \frac{v_{Rd,c} u_1 d}{\beta} = \frac{0{,}748 \times 174{,}2 \times 30}{1{,}5} \times 10^{-3} = 2{,}6 \text{ kN}$$

$$P^* = (2{,}6 - 0{,}32) \times 4 \approx 9{,}1 \text{ kN}$$

A prediction to all failure modes can be done, by comparing the loads that cause each of them to occur. In Table 8, an analysis is made for each case of surface/material loaded.

Table 8 – Actuator loads for each failure mode

Loaded surface	Failure mode	Actuator Load (kN)
Limestone	A	9,1
	B	10,1
	C	284
	D	426,6
Concrete	D*	737,8
	E	174,4
	F	40
	G	86,6
	H	64,2
	I	7,2

5.2. Tests

5.2.1. Stone plate loaded

A total of two panels were tested. One of the panels was tested only to evaluate its elastic behaviour, while the other was also tested to see a failure mode, according to the stages described in the beginning of chapter 5. Two levels of force were defined for the first stage of loading-unloading cycles: 2 kN and 4 kN. The results for the flexural test of Panel 1 are presented in Figure 11. The vertical axis refers to the actuator load (kN) and the horizontal axis refers to the average displacements (mm) measured in δ_2 and δ_4. The failure mode observed is presented in Figure 12. The results of the displacements measured in each cycle are presented in Table 9.

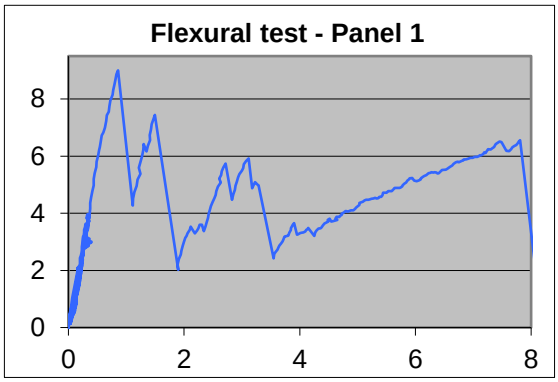

Figure 11 – Flexural test of Panel 1

Figure 12 – Failure mode observed

Table 9 – Vertical displacements

P (kN)	Displacements (mm)				
	δ_1	δ_2	δ_3	δ_4	δ_5
2	0,13	0,19	0,23	0,15	0,14
	0,12	0,19	0,23	0,17	0,15
	0,12	0,19	0,22	0,17	0.15
4	0,22	0,35	0,43	0,32	0,28
	0,21	0,35	0,42	0,37	0,29
	0,21	0,35	0,42	0,37	0,29

For the second panel loaded in the stone surface, a new level of force was considered. The results for the flexural test of Panel 2 are presented in Figure 13. The results of the displacements measured in each cycle are presented in Table 10.

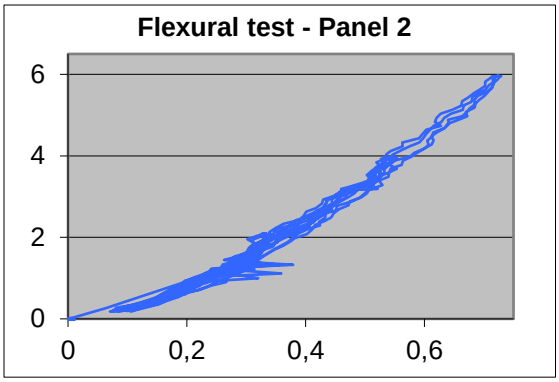

Figure 13 – Flexural test of Panel 2

Table 10 – Vertical displacements

P (kN)	Displacements (mm)				
	δ_1	δ_2	δ_3	δ_4	δ_5
2	0,29	0,35	0,36	0,32	0,28
	0,28	0,34	0,36	0,34	0,28
	0,28	0,34	0,36	0,34	0,28
4	0,43	0,54	0,58	0,55	0,42
	0,43	0,55	0,58	0,55	0,42
	0,43	0,55	0,58	0,56	0,43
6	0,56	0,73	0,77	0,72	0,53
	0,56	0,73	0,78	0,73	0,54
	0,57	0,73	0,78	0,74	0,54

5.2.2. Concrete plate loaded

For the third panel loaded in the concrete surface, the same levels of force in Panel 1 were used in this test, for the loading-unloading cycles. The results for the flexural test of Panel 3 are presented in Figure 14.

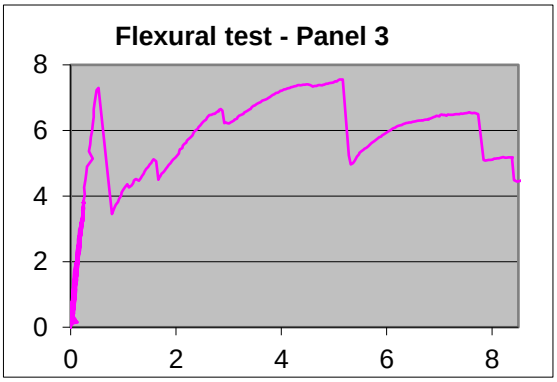

Figure 14 – Flexural test of Panel 2

The results of the displacements measured in each cycle are presented in Table 11.

Table 11 – Vertical displacements

P (kN)	Displacements (mm)				
	δ_1	δ_2	δ_3	δ_4	δ_5
2	0,16	0,1	0,13	0,11	0,1
	0,15	0,1	0,14	0,11	0,1
	0,14	0,11	0,15	0,11	0,1
4	0,24	0,24	0,31	0,25	0,18
	0,23	0,24	0,3	0,26	0,18
	0,23	0,26	0,31	0,26	0,16

The panel used in the first test (Panel 1) was reused to be tested with the same levels of force in the loading-unloading cycles. After that, the panel was loaded, until failure was verified. The results for the flexural test of Panel 1* are presented in Figure 15.

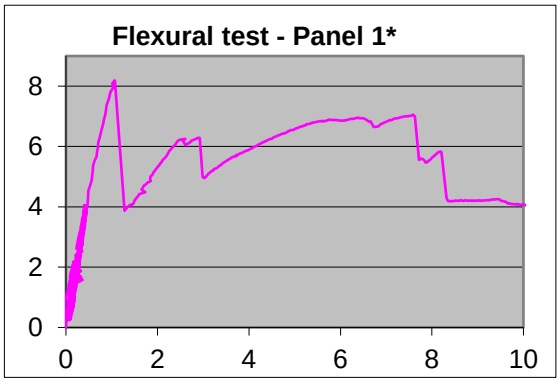

Figure 15 – Flexural test of Panel 3

6. Results analysis

According to the results obtained for the concrete characterization, the following analysis was made for three different parameters: compressive strength, tensile strength and Young modulus.

6.1. Concrete compressive strenght

The results for the concrete compressive strength show that the medium value of cubic compressive strength is 60,6 MPa. According to Appleton (2002), since the cylinder compressive strength at 28 days is approximately 80 % of the cubic strength, f_{cm} for cylinders can be estimated as 60,6 × 0,8 = 48,5 MPa. To produce a C40/50 concrete, f_{ck} must have a minimum value of 40 MPa. According to EC2, the characteristic compressive cylinder strength (f_{ck}) can be estimated as $f_{ck} = f_{cm} - 8 =$ 48,5 – 8 = 40,5 MPa > 40 MPa. This result allows to validate the concrete mixture to produce a C40/50 concrete.

6.2. Tensile strenght

The results for the splitting tensile strength of concrete ($f_{ct,sp}$) show that the medium value of splitting tensile strength is 3,27 MPa. According to EC2, a C40/50 concrete must have a minimum value of 3,5 MPa for the medium value of axial tensile strength (f_{ctm}). This parameter can be estimated with a converting factor of 0,9 (predicted by EC2): $f_{ctm} = f_{ct,sp} \times 0,9 = 3,27 \times 0,9 \approx 2,94$ MPa < 3,5 MPa. This significant difference can be explained by the presence of limestone filer in the concrete mixture. According to a study made by Parra *et al*. (2011), the presence of limestone filler in the concrete mixture of self-compacting concrete contributes to a medium decrease of 15% of the splitting tensile strength. Using that decreasing percentage, the axial tensile strength can be estimates as $f_{ctm}^* = f_{ctm} / 0,85 = 2,94 / 0,85 \approx$ 3,47 MPa ≈ 3,5 MPa. This result allows to conclude that the axial tensile strength of the self-compacting concrete produced for this panels had a decrease of 15% due to the use of limestone filer in the mixture.

6.3. Young modulus

The results for the Young modulus show that the medium value of Young modulus (E_{cm}) is 26 GPa. According to EC2, the Young modulus of a concrete produced with limestone aggregates is predicted to decrease its expected value by 10%, resulting in a value of E = 35 × 0,9 = 31,5 GPa. This difference is hard to explain since studies made to determine this concrete property have reached different conclusions. According to Persson (2001), the results for the Young modulus, shrinkage and creep remain the same for the self-compacting concretes, when compared to the same properties for

normal vibrated concretes. On the other hand, Ahmad *et al*. (2017) concluded that for the same class of concrete, the Young modulus of self-compacting concretes has a tendency of being slightly lower. Parra *et al*. (2011) share the same opinion, defending that this parameter is always lower in self-compacting concretes, with a difference of approximately 2% caused by the much higher content of the cement paste in the global mixture. However, this percentage is very low to justify the difference of 5,5 GPa between the expected value and the experimental Young modulus.

6.4. Panels flexural tests

According to the loads calculated, a comparison was made between the calculated values and the ones obtain in the flexural tests. The failure loads in each flexural test were predicted to be the two lowest loads calculated for each test (in Table 8). Those values are presented in Table 12.

Table 12 – Calculated vs experimental loads

Loaded surface	Predicted load until failure (kN)	
	Calculated	Experimental
Stone	9,2	9
Concrete	7,2	7,3

Comparing the load obtain for Panel 1 (stone surface loaded), the calculated value is very similar to the one obtained in the flexural test. This result allows to conclude that the prestress plays an important part in the conception of this panel, not only by joining all the components together (and making then work as a single panel) but also increases the resistance of the panel. Higher loads could be reached, if the prestress applied in the wires was also higher (between certain limits defined by EC2). Comparing the load obtain for Panel 3 (concrete surface loaded), the calculated value is also very similar to the one obtained in the flexural test.

7. Conclusions

i. It's possible to produce aggregate with limestone waste to be used in a mixture of a self-compacting concrete;
ii. The concrete mixture allowed to produce a C40/50 with a lower value of tensile strength and Young modulus, comparing with normal C40/50 vibrated concrete. The decreasing of the tensile strength is caused by the limestone filler used in the mixture;
iii. The displacements measured in each *LVDT* are lower in Panel 3 which allows to conclude that the flexural stiffness is slightly higher when the panel is loaded in a surface with no discontinuities.

References

Ahmad, Subhan, Arshad Umar, and Amjad Masood. 2017. «Properties of Normal Concrete, Self-Compacting Concreteand Glass Fibre-reinforced Self-Compacting Concrete: An Experimental Study». 173: 807–13.

Costa, António, and Júlio Appleton. 2002. «Estruturas de Betão I, Parte II - Materiais».

Ferreira, Luís Filipe Brandão, Doutor Eduardo Nuno Brito Santos Júlio Co-Orientador, Doutor Hugo Sérgio Sousa Costa Co-Orientador, e Mestre Paulo Maranha Nunes Tiago. 2015. «Painéis de Fachada Prefabricados em Betão Eco-Eficiente Ativado Tese especialmente elaborada para obtenção do Grau de Doutor em Engenharia Civil Tese Provisória».

Parra, C, M Valcuende, and F Gómez. 2011. «Splitting tensile strength and modulus of elasticity of self-compacting concrete». *Construction and Building Materials* 25(1): 201–7.

Persson, Bertil. 2001. «A comparison between mechanical properties of self-compacting concrete and the corresponding properties of normal concrete». 31.